Search for strange baryonium states in $\bar{p}d$ interactions at 8.9 GeV/c

G. H. N. Shoemaker,* Winston Ko, W. Michael,† R. L. Lander, D. E. Pellett, P. M. Yager, J. R. Smith, M. P. Cain, K. Maeshima, and M. C. S. Williams
Physics Department, University of California, Davis, California 95616
(Received 30 June 1986; revised manuscript received 23 September 1987)

A search for SU(3) manifestly exotic $Q^2\bar{Q}^2$ baryonium states in antiproton-deuterium interactions was carried out at the SLAC 40-in. hybrid bubble-chamber facility. The $I=\frac{3}{2}$, $S=1$ channel, X^-, produced in conjunction with a forward produced neutral antikaon was studied. Such X^- states would decay into an antihyperon and a baryon. The fast forward $\bar{K}^0$ was detected in a three-view segmented calorimeter placed downstream of the bubble chamber and used as part of the trigger. Upper limits of 0.50–1.63 μb are reported for the $X^-\to\bar{\Lambda}n\pi^-$, $\bar{\Sigma}^-n$, $\bar{\Lambda}p\pi^-\pi^-$, $\bar{\Sigma}^-p\pi^-$, $\bar{\Sigma}^{\pm}n\pi^{\mp}\pi^-$ exclusive channels based upon ≤ 13 events per channel.

I. INTRODUCTION

There has been considerable interest in the search for hadrons having quantum numbers not explainable in terms of the conventional models of hadron structure.[1] Indeed, a consistent view of hadron dynamics may require states with "exotic" hadron structure. For example, duality in the baryon-antibaryon amplitude may necessitate $Q^2\bar{Q}^2$ states.[2] In the dual-topological-unitarization approach to hadron physics, they are regarded as ordinary as mesons and baryons.[3] In addition, there are no dynamical reasons to exclude exotic states. More complex quark configurations could, in principle, exist in color-singlet states.

The $Q^2\bar{Q}^2$ (M_4) structure is the simplest of these exotic configurations that has a color-singlet state. Because the total number of spin-orbital angular momentum degrees of freedom in M_4 states is much greater than for normal mesons, such states are expected to be broad and plentiful and their resonances hard to identify. However, some models do specify M_4 states which could be quite stable and isolated in the mass spectrum.[4]

The color-chemistry model of Chan and Høgaasen[5] groups the quarks into a diquark-antidiquark arrangement where each of the diquarks are in a relative S-wave state. Two possible arrangements that can give color-singlet states emerged and were designated T-diquonium ($3\otimes\bar{3}$) and M-diquonium ($6\otimes\bar{6}$). These diquonium states have three possible decay modes: baryon-antibaryon $B\bar{B}$ (baryonium), meson-meson MM (mesonium), and meson cascade MM_4. T-diquonium couples readily to BB in the high l states. On the other hand, M-diquonium couples to $B\bar{B}$ only weakly, and for $l\leq 2$ may not be sufficiently stable against MM decay.[6]

An initial search would appear to be preferred for T-diquonium since its decays have the distinctive baryon-antibaryon signature. By contrast, the M-diquonium states would have a large multimeson background which could hide a diquonium resonance. Also the mesonium decays for M-diquonium states which are superallowed by the Okubo-Zweig-Iizuka (OZI) rule are expected to be quite broad since the diquonium configurations with strongly overlapping wave functions are inherently unstable.[7] We thus concentrate on baryonium processes.

Nicolescu has presented a comprehensive survey of the evidence for exotic exchange processes where the baryonium exchange hypothesis is favored.[8] Strong candidates at present for narrow baryonium states are the 2020-MeV resonances reported by Azooz *et al.*[9] Two resonances of widths 14–20 MeV were seen at the 1-μb level for

$$\bar{p}p\to(p_f\bar{n})\pi^+\pi^-\pi^- \quad (6\text{ GeV}),$$

$$\bar{p}p\to\pi_f^+(\bar{p}n)\pi^+\pi^- \quad (9\text{ GeV}),$$

triggered by forward-produced protons and pions, respectively. These results suggest a genuine cryptoexotic $N\bar{N}$ multiplet with isospin 1.

More interesting, however, were the signals at 3.1 GeV/c^2 recently reported by Bourquin *et al.*[10] Three narrow and coincident peaks ($\Gamma<30$ MeV/c^2) were observed in the channels

$$U^+:\ \Lambda\bar{p}\pi^+\pi^+,$$

$$U^0:\ \Lambda\bar{p}\pi^+\pi^+\pi^-,$$

$$U^-:\ \Lambda\bar{p}\pi^+\pi^-,$$

at the 1.2–4.8-μb level. If these final states are the result of strong decays, then the U^+ particle has the SU(3) exotic quantum numbers $B=0$, $Q=1$, and $S=-1$, and must contain at least four quarks $sud\bar{d}$. It has been convincingly argued that weak decays are improbable and that the most natural identification of these states is as an $I=\frac{3}{2}$ strange baryonium multiplet.[11] However, the existence of a U^{--} state is crucial to this interpretation and must be experimentally established. (The decay mode $U^{--}\to\Lambda\bar{p}\pi^-$ failed the trigger criterion in the experiment above.)

Direct production of manifestly exotic states is ruled out in MB reactions by planarity constraints,[12] and in $B\bar{B}$ processes by lack of the required exotic quantum numbers in either $p\bar{p}$ or $\bar{p}n$ combinations. Some experi-

ments attempted invariant or missing mass fits for exotic mesons produced in the forward direction.[13] More recently, backward processes have been studied experimentally;[14] and each of the allowed planar processes have been surveyed with the exception of the reaction channel to be considered in the present paper.

II. SELECTION OF THE REACTION CHANNEL AND EXPERIMENT

Our experiment studies the production of SU(3) exotic T-diquonium states in the reaction $\bar{p}n \to \bar{K}^0 X^-$ at the Stanford Linear Accelerator Center (SLAC) using the SLAC hybrid bubble-chamber facility (SHF) modified by the addition of a hadron calorimeter downstream. The incident-beam momentum was 8.9 GeV/c and the minimum K^0 triggering energy was 3.5 GeV. The experiment was sensitive to masses in the range from 2.2 to 3.6 GeV/c^2. An average resolution of 40–110 MeV/c^2 (depending upon the channel) was obtained from kinematic fitting. The search was restricted to $Q=-1$ and $S=+1$ baryon and antihyperon decay channels, represented by

$$X^- \to \bar{\Sigma}^- N ,$$
$$\to \bar{\Sigma}^- \Delta^0 ,$$
$$\to \bar{\Lambda} \Delta^- ,$$
$$\to \bar{\Sigma}^0 \Delta^- ,$$

(where $\bar{\Lambda}$, N, $\bar{\Sigma}$, Δ represent the baryon multiplets with $I=0, \frac{1}{2}, 1, \frac{3}{2}$, respectively) and having no more than one missing neutral.

The selection of this particular reaction channel was motivated by the following considerations.

(1) Asymptotic planarity of the S matrix and kinematic considerations favor a production mechanism $B\bar{B} \to MM_4$ (see Fig. 1). Ignoring gluon exchange, the color-singlet hypothesis would also favor T-diquonium in this production mechanism.[15] Therefore,

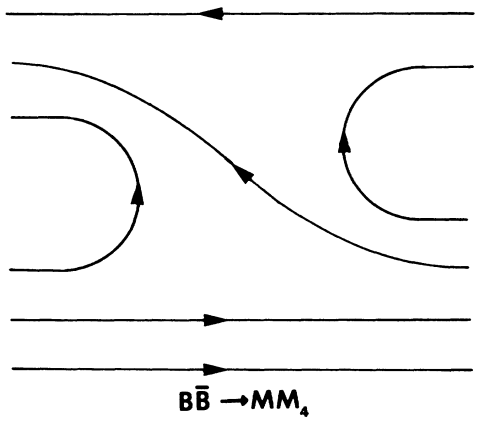

FIG. 1. Planar quark-line diagram for SU(3) exotic $QQ\bar{Q}\bar{Q}$ states in $B\bar{B} \to MM_4$.

$$\bar{p}n \to \pi^+ Z^{--}$$

and

$$\bar{p}n \to \bar{K}^0 X^-$$

emerge as the most promising channels. If the enhancement of the $\bar{p}n \to \pi^+ Z^{--}$ cross section is not too great (see Fig. 2), the reduced background associated with the $\bar{p}n \to \bar{K}^0 X^-$ reaction[16] could favor searches in that channel. The $\bar{p}n \to \pi^+ Z^{--}$ reaction channel has already been studied,[17] so our search is complimentary, providing the opportunity to conclude the survey of the planar diagrams at the 1-μb level.

(2) The diquark model and color-symmetry arguments indicate that the T-diquonium ($M_4 \to B\bar{B}, B\bar{B}M, \ldots$) processes should dominate for backward production of M_4 (Ref. 18). Baryonium decays also appear to be favored over mesonium decays, especially for high-l states.[19]

(3) An examination of the flavor-SU(3) symmetry of the exotic system will allow us to write

$$3 \otimes 3 \otimes \bar{3} \otimes \bar{3} = 36 \otimes 18 \otimes 18 \otimes 9$$
$$= (27 \otimes 8 \otimes 1) \otimes (10 \otimes 8) \otimes (\overline{10} \otimes \bar{8}) \otimes (8 \otimes 1) . \quad (1)$$

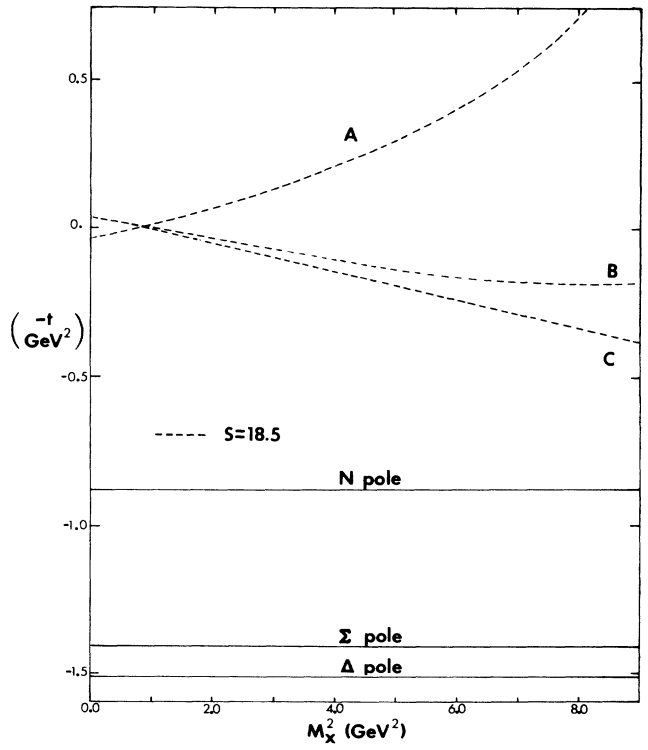

FIG. 2. Proximity of reaction channels to exchange poles using a Chew-Low plot. The kinematic boundaries are indicated by dotted lines for (A) $\pi^- n \to p Z^{--}$, (B) $\bar{p}n \to \bar{K}^- X^-$, and (C) $\bar{p}n \to \pi^+ Z^{--}$. An enhancement is indicated for (C) by the proximity of the boundary to its corresponding pole and is approximately an order of magnitude larger than (A).

The manifestly exotic quantum numbers are found in the **27**, **10**, and $\overline{\mathbf{10}}$ multiplets. The Z^{--} state can lie only in the **27** multiplet; our state X^- lies in both decuplets, however. For a given value of l, states in the **36** multiplet reside at M^2 values approximately 1 GeV^2 higher than the corresponding **18** multiplet states. Therefore, SU(3) exotic states found in either the **10** or $\overline{\mathbf{10}}$ multiplets will likely lie closer to threshold than those in the **27** multiplet for given values of l.[20] The widths of these T-diquonium resonances are expected to fall within the normal range associated with hadronic decays. Resonances near the mass threshold, however, *may be very narrow due to kinematic suppression.*

(4) The bubble chamber, because of its large angular acceptance and the ionization information available for low-momentum charged particles, is suitable for studying the backward production of M_4. The strange-baryonium channel (X^-) is expected to decay preferentially to baryon-antihyperon, thereby supplying a distinctive signature in a bubble chamber. The acceptance for and identification of the slow-moving antihyperons are quite good in the bubble chamber.

In addition, our X^- state has the opposite quark composition relative to the U^+ resonance discussed earlier (see the Introduction). Therefore, confirmation of the strange baryonium hypothesis for the U multiplet is possible with this reaction channel if narrow signals are observed and yield a Regge trajectory with an integral J value corresponding to 3.1 GeV/c^2.

III. CHOICE OF TRIGGER

To facilitate the production and identification of X^- states, we chose kinematic conditions such that $\bar{K}^0$ be well separated in rapidity space from the X^-. We required a minimum rapidity gap of one-half unit, and obtained a condition on the produced mass M: $M^2 < s/\sqrt{e}$. For our beam energy, this corresponds to a mass upper limit of approximately 3.6 GeV. (The lower limit of 2.2 GeV is set by the $\bar{\Lambda} n \pi^-$ threshold.) The condition on the rapidity also places the K^0 trigger energy threshold approximately at 3.5 GeV. A segmented, hadron calorimeter[21] can be readily used to form a K^0 trigger for the X^- channel. The angle of the $\bar{K}^0$ can be adequately reconstructed to yield an unconstrained fit on the decays of interest. The energy resolution of the calorimeter affords an acceptably sharp cut on the forward-going momentum, and a loose but adequate constraint on momentum in the kinematic fit. The K^0's easily escape the chamber and provide essentially unbiased angular acceptance. A calorimeter of moderate size and density can be expected to convert virtually all of the K^0's and give an energy resolution of $\simeq 50\%/\sqrt{E}$ (E in GeV). Significant contributions to the trigger rate, however, are expected from charge-exchange processes which produce an $\bar{n}$ in the forward direction. These $\bar{n}$ events can be easily rejected in the scanning because they cannot contribute to the distinctive signature of the X^- decay.

IV. THE EXPERIMENTAL SETUP

A. Experimental apparatus

Figure 3 exhibits the setup of the apparatus for our experiment. The primary $\bar{p}$ beam is collimated to transmit $\Delta p/p = 1\%$ full width at half maximum. For the rf separator operating at 8.9 GeV/c, the average $\bar{p}$ composition of the beam was typically 50–60 %.

Positioned just upstream of the bubble chamber were the beam Čerenkov counter CB and the hodoscope BH which provides a crude vertical position measurement of the beam tracks. A beam track was defined by the coincidence $S1 \cdot \mathrm{BH}$, with pulse widths typically 4-nsec wide. The $\bar{p}$ signal was defined by the logic $S1 \cdot \mathrm{BH} \cdot \overline{\mathrm{CB}}$. (Further details are given in Sec. IV B.)

There were four proportional wire chamber planes upstream of the bubble chamber to provide beam position information for resolving triggering ambiguities and adjusting the measured beam parameters. The bubble chamber had 110-cm diameter and 43-cm depth and used three stereo views. The bubble-chamber magnet was operated at the maximum field strength of 26.225 kG, but with a low bubble density (8 bubbles/cm) allowing particle identification by track ionization for momenta less than 1.5 GeV/c.

Immediately downstream from the bubble chamber were three proportional wire chambers (PWC's) to measure track positions and momenta of fast outgoing charged particles (Fig. 3). Placed 4 m downstream from the bubble-chamber center were a collection of three counters: a beam veto counter BV, a veto counter for outgoing charged tracks $V1$ and $V2$ (CV), and the calorimeter.

The BV counter was a narrow scintillation counter (≈ 6 cm $\times$ 12 cm) matched to the dimensions of the beam and placed to intercept and veto the noninteracting beam after it is deflected by the magnet. Another veto counter CV was placed in front of the calorimeter to ensure that the calorimeter triggered only on neutral particles. Placement of the calorimeter permitted adequate angular acceptance for the K^0 while minimizing both the acceptance window of the veto counter for outgoing charged particles and the effects of the bubble-chamber fringe field on the electronics of the calorimeter.

The calorimeter consisted of alternating layers of absorber and scintillator to provide three views of energy deposition. It was segmented in both the longitudinal (X) and transverse (Y and Z) directions (Fig. 4). Energy deposition profiles allowed reconstruction of the location of the neutral hadron initiating the shower and its shower development. The calorimeter was calibrated using pion beams at 7 and 9 GeV/c to ensure uniform response in both the transverse and longitudinal readouts for hadron showers initiated almost anywhere inside the calorimeter. (Further details of the calorimeter design and calibration method can be found elsewhere.[22])

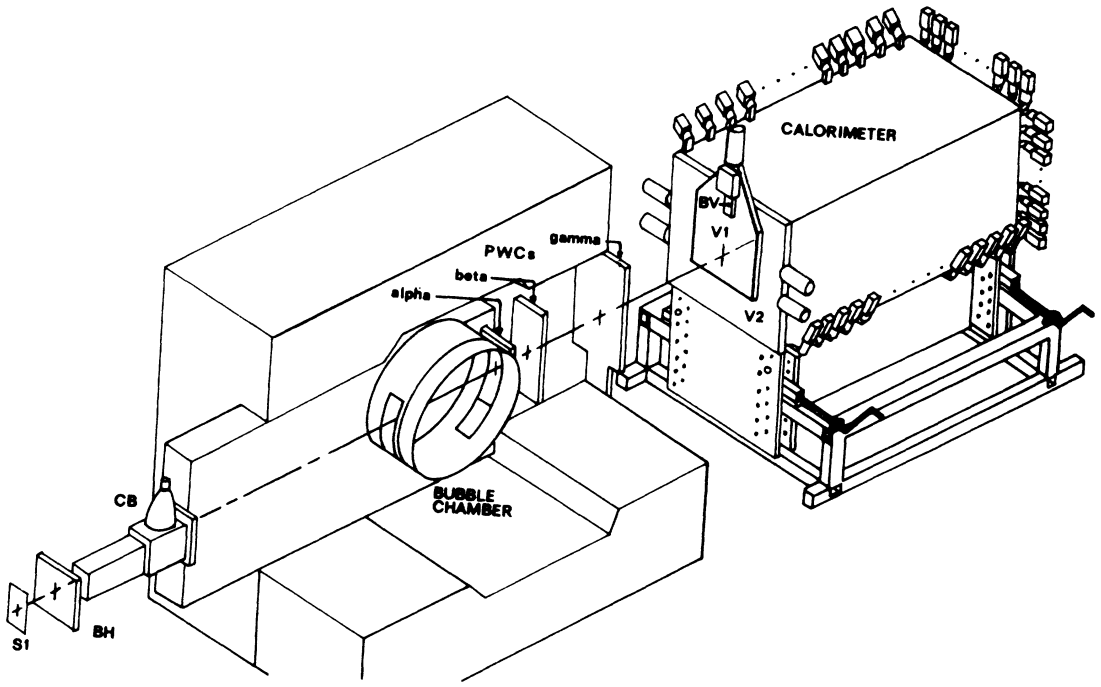

FIG. 3. Schematic of the modified SHF. $S1$ and BH represent the scintillator counter and beam hodoscope, respectively, for beam definition; CB is the beam Čerenkov counter for particle identification; the PWC chambers define track points for the momentum determination of high-energy particles; BV is the beam veto counter to ensure triggering on events with beam interactions; and $V1$ and $V2$ are veto counters to ensure triggering on neutral particles.

B. The trigger

Our trigger consisted of both a hardware and software component. The scintillation counters and summed output from the calorimeter triggered the main processor in less than 1 μsec. A software algorithm processed this information from the calorimeter and PWC's to trigger the bubble-chamber cameras (a time typically on the order of 3–3.5 msec).

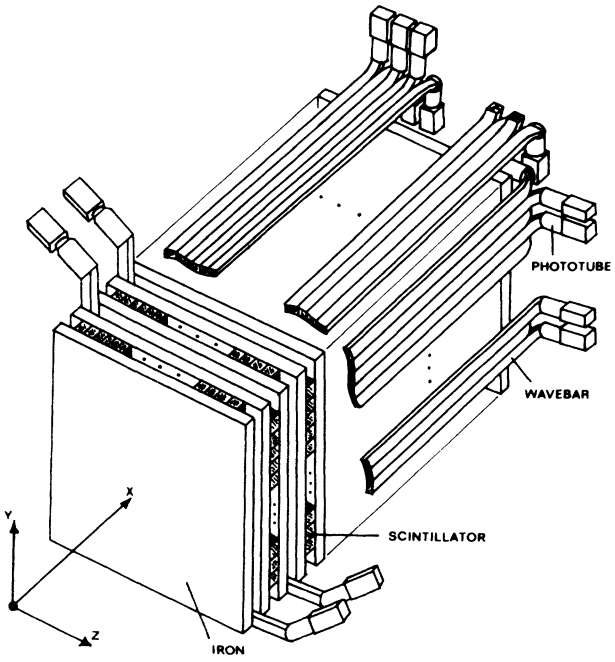

FIG. 4. Schematic view of the calorimeter. The numbering of the tubes is sequential and increasing with the coordinate values as indicated on the diagram.

The hardware trigger was defined by $S1\cdot BH\cdot\overline{CB}\cdot\overline{BV}\cdot\overline{CV}\cdot\sum X_{min}$, where $\sum X_{min}$ represents a lower bound on the sum of discriminated phototube pulse heights for the longitudinal planes (X) of the calorimeter. In other words, we required that there be a $\bar{p}$ defined by the upstream counters ($S1\cdot BH\cdot\overline{CB}$), an interaction in the bubble chamber (BV), a veto on charge particles entering the calorimeter (CV), and a minimum deposition of energy in the calorimeter ($\sum X_{min}$). The discriminated pulses from the X planes were channeled through a linear adder circuit to compute $\sum X$. This "soft" energy cut was obtained by adjusting appropriately the threshold level on a discriminator receiving the summed X output signal.

Under normal experimental conditions, the downstream tagging apparatus will allow two triggers per beam pulse; however, this cannot be permitted with our neutral trigger since more than one primary interaction in the chamber would make the assignment of the neutral track ambiguous and the energy deposited in the calorimeter would result from two events. So each $S1\cdot BH$ trigger initiated a 240-nsec gate (of which 100 nsec was pretrigger) suppressing the trigger for coincidences with other neighboring $S1\cdot BH$ signals.[23]

The software algorithm tested four conditions: (1) Two of the four upstream planes were required to have one and only one hit; (2) a lower cut on $\sum X$ [now the sum of the actual pulse heights read into the analog-to-digital-convertor (ADC) channels] was imposed; (3) the number of $S1\cdot BH$ counts per beam spill was required to

be <10; (4) we required two of the planes in the α PWC to register ≤ 2 hits. Condition (1) permitted beam identification with less ambiguity and improved its position and momentum reconstruction. Condition (2) imposed the energy cut. The final two conditions were introduced to reduce the picture rate by discarding obvious unwanted events. The specification of the PWC multiplicity cut (4) was determined by comparing the results of acceptance Monte Carlo calculations for various PWC algorithms for 62 000 frames of data taken with an unbiased trigger at the beginning of the run cycle.

V. DATA REDUCTION WITH THE SHF AND CALORIMETER

A. Bubble-chamber analysis

The film for this experiment contained 4×10^5 triplets plus 2×10^3 triplets exposed for calibration purposes. Event-selection criteria required straight interacting beam tracks with "vees" pointing to the primary or a secondary vertex and/or "kinks" exhibiting incoming track lengths and ionization characteristics of a Σ decay. We demanded that these PWC data be properly matched to the beam track in the chamber and that the number of events not exceed one for any given frame. Approximately 10% of the film was rescanned to determine the scan efficiency for locating vees or Σ's.

Events selected by the scanners were sent directly to the measuring machine, which was equipped with a three-view film drive and which could be operated with a precision of one micron in the film plane. The guidance program ARIEL,[24] minimized track matching mistakes by allowing a given track to be measured successively in three views before the measurer had to divert his attention to another track.

The film setting error for our experiment was 5 μm, as determined by examining the distribution of confidence level for the successful K^0 fits and the "pull" quantities for ϕ, s, and k of the outgoing tracks. The rms deviation of measured versus fitted points in the film plane (frms) shows little variation with respect to particle type and peaks typically around 8 μm. Our experiment required searching for exotic channels by utilizing kinematically fitted data. For this reason we had the measurer skip events with >6 prongs (including the spectator proton) at the primary vertex.

B. Neutral tracks from calorimeter data

The calorimeter was segmented in all views and calibrated to ensure approximately equal response over the entirety of the detector. This makes it possible, in principle, to supply the kinematic track parameters ϕ, s, k, and their corresponding errors for our neutral triggering particles in addition to the usual energy deposition.

The average energy deposition is known to be proportional to the sum of the pulse heights of all of the individual channels[25] and we write

$$E\approx\alpha_1\left[\sum_{i=1}^{N}A_i\right], \tag{2}$$

where N represents all 122 channels and A_i is the ADC reading for the ith bin. Over a range ±40 cm from the center, this total sum was quite uniform over the transverse coordinates of the calorimeter.[26] The gain coefficient α_1 is determined by comparing the values for our noninteracting-beam data to the measured pulse-height sums. Our expected error was dominated by sampling and is approximately independent of shower location. We obtained

$$\sigma/E=52\%/\sqrt{E}\ \ (E\text{ in GeV}) \tag{3}$$

from the noninteracting-beam data.

The centroid values of the pulse heights in each direction are normally used to assign coordinates for the constructed end point. However, for our purposes the median provided a better, less biased estimate of $\langle x\rangle$ than the actual arithmetic mean since a large fraction of events had showers with poor containment through the sides of the calorimeter.

For most showers, the error on the shower location is dominated again by energy sampling, and so the errors have approximately a $1/\sqrt{E}$ dependence for a given shower width,

$$\sigma\simeq\frac{KS}{\sqrt{E}}\ , \tag{4}$$

where K is the energy sampling coefficient, S is the standard deviation of the shower pulse-height distribution for a given X, Y, or Z profile, and E is the energy sampled (in GeV).

For well-contained showers, S can be determined in the usual way. However, for poorly contained showers, we developed an algorithm which could be applied independently of the shower containment. (Further details of this analysis can be found elsewhere.[27])

C. Kinematic-fitting procedure

To determine if the event was likely to contain a strange particle, the vees and kinks were fitted with the usual strange-particle fitting hypotheses. Poorly fitting Σ candidates were rejected, but positive identification required compatibility with the ionization information.

Events with at least one successful strange-particle secondary-vertex fit were subjected to further processing. For the vees, a three-constraint (3C) fit with confidence level $\geq5\%$ was required. The energy resolution of the calorimeter restricted our fits to the one missing neutral hypotheses. Fits with and without the calorimeter track were tried to check whether the calorimeter deposition could have resulted from processes other than forward-going K^0's. A confidence-level cut for passing event hypotheses was 5%.

D. Selection of the *T*-diquonium event candidates

Events included in our T-diquonium analysis first had to have adequate track information. The beam track was required to fit both the nominal values for p, λ, ϕ, and the PWC information from the upstream chambers at a confidence level of 0.1% or greater. Because of

some inefficiencies in the on-line data acquisition, some events did not have beam tagging information available and were rejected. Further, we rejected beam tracks which fit only to the nominal TVGP beam values unless there were PWC fits in the downstream chambers for outgoing tracks. The PWC chambers provided the only unambiguous signals linking the Čerenkov counter information with the measured beam track. It was particularly important for the weakly constrained 1C fits that the beam particle identity be accurate to keep the background to a minimum.

Confidence levels of $\geq 5\%$ were required for fitting the secondary vertices $\bar{\Lambda}$ (3C) and $\bar{\Sigma}^{\pm}$ (1C). The rest of the event was subject to a kinematic fit covering all tracks and vertices corresponding to one or more of the hypotheses

$$\begin{aligned}\bar{p}d &\rightarrow p_S \bar{K}^0 \bar{\Lambda} n \pi^- \\ &\rightarrow p_S \bar{K}^0 \bar{\Sigma}^- n \\ &\rightarrow p_S \bar{K}^0 \bar{\Lambda} p \pi^- \pi^- \\ &\rightarrow p_S \bar{K}^0 \bar{\Sigma}^{\pm} n \pi^{\mp} \pi^- \\ &\rightarrow p_S \bar{K}^0 \bar{\Sigma}^- p \pi^- ,\end{aligned}$$

where p_S refers to the spectator proton. Again, passing events required fits of a confidence level $\geq 5\%$.

Some additional comments are in order regarding the selection procedure.

(1) We could not tolerate the loss of one constraint on the fitting of the above 1C channels unless it was due to the loss of the calorimeter momentum information, since this value was already poorly determined.

(2) Events were checked with fitting hypotheses having no K^0 required in the calorimeter to see if the calorimeter could have been triggered by one of the remaining tracks in the event. This could occur, in principle, in one of three ways: (a) interaction events in the bubble-chamber window, (b) false triggers by charged tracks not vetoed by the veto counter, or (c) triggers associated with other missing neutrals.

(3) All accepted fitting hypotheses had to be consistent with the ionization information obtained from the bubble chamber. Each event was checked on the scan table and particle identity was assigned by comparing the visual ionization with the values determined by the fitted track parameters. The identification criteria were loose enough so that tracks could be ambiguously assigned several possible identities rather than risk misidentification.

E. Normalization

Table I gives information required for normalizing the cross sections (or upper limits). Here we present a summary of the most important considerations that were involved in these calculations.

The beam luminosity was determined from the scalers which monitored the trigger counters. The total number of $\bar{p}$'s passing through our experimental apparatus during the run cycle was found to be $\approx 1.7 \times 10^7$. This number was adjusted to correct for the inefficiencies associated with the beam scintillation and Čerenkov counters and includes the camera dead time. The number of interacting beam particles was estimated for a deuterium-filled chamber operating at 20 K and 10 atm pressure. The fiducial volume for primary interactions allowed by the scan rules is $\simeq 84\%$ of the visible volume of the bubble chamber. If we also include the correction for $\bar{K}^0$ interactions in deuterium but ignore trigger dead time, we can set for $\bar{p}n \rightarrow K^0$ (inclusive) interactions a value of 29.3 ± 0.8 events/μb for our experiment.

TABLE I. Summary of corrections for the cross-section normalization.

Beam interaction		0.840 ± 0.010
Trigger particle interaction		0.102 ± 0.013
Beam-tagging efficiency		0.738 ± 0.024
Calorimeter/fast-trigger dead time		0.677 ± 0.002
Calorimeter efficiencies	1C events	0.968 ± 0.003
	3C events	0.926 ± 0.019
Scanning efficiencies	$\bar{\Lambda}$	0.915 ± 0.011
	$\bar{\Sigma}$	0.977 ± 0.016
Data-processing efficiencies	$\bar{\Lambda} n \pi^-$	0.930 ± 0.010
	$\bar{\Sigma}^- n$	0.758 ± 0.036
	$\bar{\Lambda} p \pi^- \pi^-$	0.844 ± 0.018
	$\bar{\Sigma}^- p \pi^-$	0.699 ± 0.040
	$\bar{\Sigma}^- n \pi^{\mp} \pi^-$	0.699 ± 0.040

As previously mentioned, multiple beam interactions in the bubble chamber during a given beam pulse would have presented difficulties in our analysis. It was therefore necessary to set up a gate to veto unresolved beam particles. This triggered dead-time value (which in Table I represents the percentage of beam particles that survive) was determined using a Monte Carlo calculation which simulated the structure of the beam spill and imposed the gating constraints. Dead time due to the processing of the fast-trigger algorithm was insignificant. Each time the fast-trigger requirements were satisfied, however, the software algorithm was activated; so each beam particle satisfying the fast trigger requirements killed the remainder of the beam spill. Our value (see Table I) includes this correction.

The efficiency of our beam-fitting procedure was defined by the fraction of beam tracks accepted out of a total sample of good beam tracks (i.e., those known to have been associated with the trigger). This sample was obtained by considering noninteracting-beam data and selecting events with $\geq 5\%$-confidence-level fits in the downstream PWC's alone. (This condition ensured that we had located the right beam track.) The distribution for fits in the upstream chambers were then examined independently for events which passed and failed the downstream PWC fitting criteria. The distributions suggested a confidence level cut of 0.1%, for which the fraction of good beam tracks lost was 25.2%.

Our event-selection criteria included the requirement of kinematic fits to the whole event. The fits fell into two categories: those with and those without missing neutrons, corresponding to 1C and 3C fits, respectively.

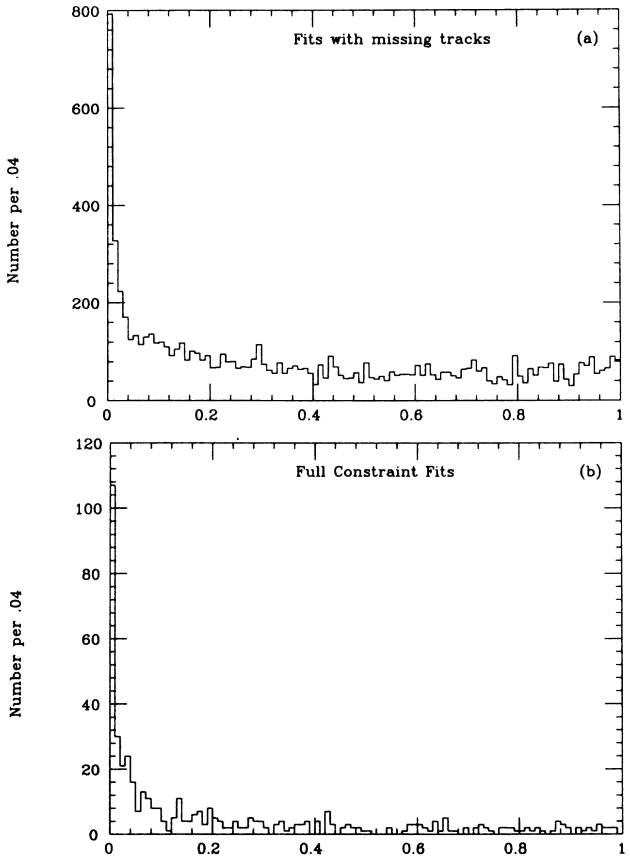

FIG. 5. Confidence levels for (a) 1C and (b) 3C fitted events.

(The calorimeter track parameters are used in both of these fits.) The confidence-level distribution (Fig. 5) are reasonably flat with a slight rise toward the low end. Since they only indicate a slight underestimation of the errors, a reasonable approximation of the number of good events in the background peak can be obtained by extrapolating a polynomial curve (fitted over the data from 0.15 to 1.0) back to 0.0. We choose a confidence-level cut at 5%. The calorimeter efficiency is computed by comparing the above acceptance value to the expected value for this cut (see Table I).

F. Trigger acceptances

The acceptance of our trigger for each of the exclusive channels of interest was determined by using a Monte Carlo calculation. A distribution of t values for the K^0 inclusive processes to be used in the calculation was plotted (Fig. 6) using 1C multivertex kinematic fits with the calorimeter track identified as a K^0. We can justify the use of the K^0 inclusive data for our estimation by noting that all planar diagrams with a K^0 fast forward on $\bar{p}n$ scattering require a Σ hyperon exchange (assuming single-particle processes dominate).[28] Our Monte Carlo program estimated acceptance values for the following additional considerations (please refer to the first column of Table II).

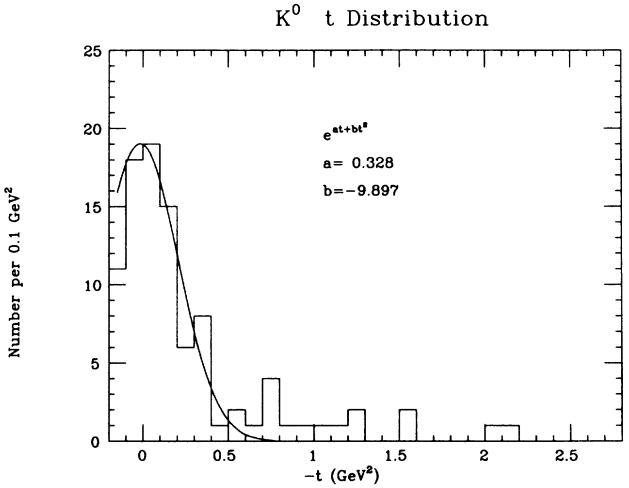

FIG. 6. t distribution for K^0 inclusive data sample. The parametrization and resulting curve determined from these data and used in the Monte Carlo analysis are also shown.

(1) Events with K^0 reaching the fiducial volume of the calorimeter. The acceptance window was set 5 cm away from the sides of the calorimeter.

(2) Events with visible strange-particle decays having primary interactions within the fiducial volume of the bubble chamber. The secondary vertices were sufficiently far from the chamber wall to allow a good determination of the track parameters for all of the charged tracks in the event.

(3) Events with no signals produced in the veto counter CV. Signals in the CV counter can result from the charged particles originating from the M_4 decay, as is frequently true for the higher-momentum protons and/or $\bar{p}$'s. The calculation takes into account the measured efficiency of the veto counter CV.

(4) Events with only one neutral particle within the acceptance window of the calorimeter. This problem is

TABLE II. Monte Carlo acceptances for the $S=1$ T-diquonium channels (2000 events). Each of the entries in the first column are explained in Sec. V F of the text.

	$\bar{\Lambda}n\pi^-$	$\bar{\Sigma}^-n$	$\bar{\Lambda}p\pi^-\pi^-$	$\bar{\Sigma}p\pi^-$	$\bar{\Sigma}^{\pm}n\pi^{\mp}\pi^-$
K^0 acceptance	0.957	0.957	0.957	0.957	0.957
Fiducial volume	0.826	0.972	0.843	0.969	0.984
Veto counter	0.844	0.989	0.814	0.877	0.974
Single particle	0.870	0.797	1.000	0.875	0.633
α PWC	0.974	0.998	0.839	0.987	0.980
Overall	0.564	0.732	0.552	0.702	0.569

TABLE III. Topological distribution for events with ≤ 4 prongs. (A visible spectator proton is counted as a prong.)

Topology	1 Prong	2 Prong	3 Prong	4 Prong
1 vee	374	262	282	146
2 vees	55	44	21	21
1 positive kink	0	5	26	28
1 negative kink	70	68	88	42
1 vee, 1 positive kink	0	0	13	8
1 vee, 1 negative kink	56	37	42	9

particularly acute for our T-diquonium channels where the neutrons and $\bar{n}$'s typically have momenta $\geq 40\%$ of the momentum of the K^0.

(5) Events satisfying the downstream PWC requirements. Our trigger algorithm required ≤ 2 hits in two of the planes of the α chamber.[29] This cut was imposed to eliminate events with three or more forward-going charged particles from the data sample. The efficiency for vetoing ≥ 3 charged tracks crossing the α chamber is found to be close to 100%, but accidentals can cause some legitimate events to be vetoed as well.

VI. RESULTS FOR THE STRANGE T-DIQUONIUM SEARCH

The events with visible strangeness represent about 2–3 % of the total sample. In Table III, we present a topological breakdown for these events having ≤ 4 prongs, satisfying the beam-fitting criteria, and having all tracks processed successfully. The K^0 and Λ particles are produced predominantly at low momentum forward in the laboratory system. However, the Λ's are produced backward in the center-of-mass system, while

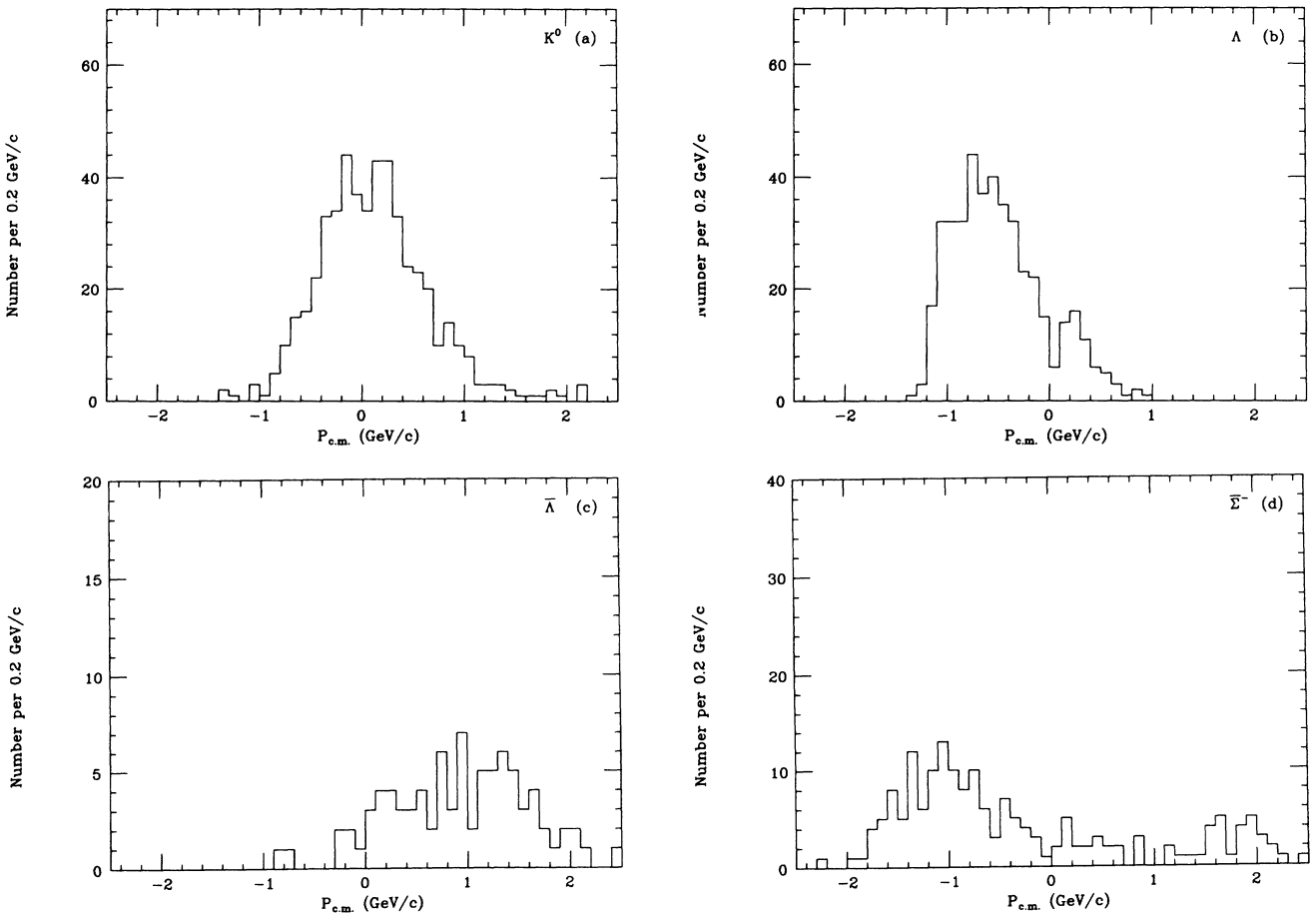

FIG. 7. Longitudinal component of c.m. momentum for strange particles visible in the bubble chamber. (a) K^0; (b) Λ; (c) $\bar{\Lambda}$; (d) $\bar{\Sigma}^-$.

TABLE IV. Topological distribution of $\bar{\Lambda}$ and $\bar{\Sigma}$ events with ≤ 4 prongs.

Topology	$\bar{\Lambda}$	$\bar{\Sigma}$
1/2 prong	62	96
3/4 prong	23	80

the K^0's are evenly distributed forward and backward [see Fig. 7(b)]. The $\bar{\Lambda}$'s are seen to be predominantly forward in the c.m. system [Fig. 7(d)]. These phenomena are all consistent with the dominance of single-particle-exchange processes.

For the $\bar{\Sigma}$ candidates we required successful 1C fits to the decay vertex and demanded that the fitted values for ionization be consistent with the values observed in the bubble chamber. Many $\Sigma/\bar{\Sigma}$ ambiguities were not resolved and become part of the background. For events with $\bar{\Lambda}$ and $\bar{\Sigma}$ candidates we present the charged multiplicities (which includes the spectator proton) in Table IV. Applying the event-fitting criteria discussed in Sec. V C, each of the three- and four-prong channels have fewer than 4 events. However, in the $\bar{\Lambda}n\pi^-$ and $\bar{\Sigma}^-n$ channels, there are 19 and 32 events, respectively.

For these two channels we present the distribution of the production angle cosine in the center-of-mass frame (Fig. 8). We now introduce a kinematic cut (accepting only events with the K^0 trigger momentum >3.5 GeV/c) to isolate that part of the phase space where the T-diquonium would be backward produced and isolated in rapidity from the K^0. The events surviving this cut, indicated by the shaded histograms in Fig. 8, clearly show evidence of single-hyperon-exchange processes, as expected.

Finally, in Fig. 9 are plotted the invariant masses for these two channels for the events surviving the kinematic cut. Neither of these distributions exhibit any significant signal, as can be seen by comparison with the calculated phase-space backgrounds superimposed on each histogram.[30] The bin widths of 40 MeV/c^2 and 100 MeV/c^2 corresponded approximately to the average mass resolutions (σ) for the $\Lambda n\pi^-$ and $\bar{\Sigma}^-n$, channels, respectively. The difference in the mass resolution for the two channels is due to the poorer measurement of the $\bar{\Sigma}$ momentum from the bubble-chamber data.

To estimate the upper limits we chose a four-bin-wide mass interval (i.e., four times the average σ for individu-

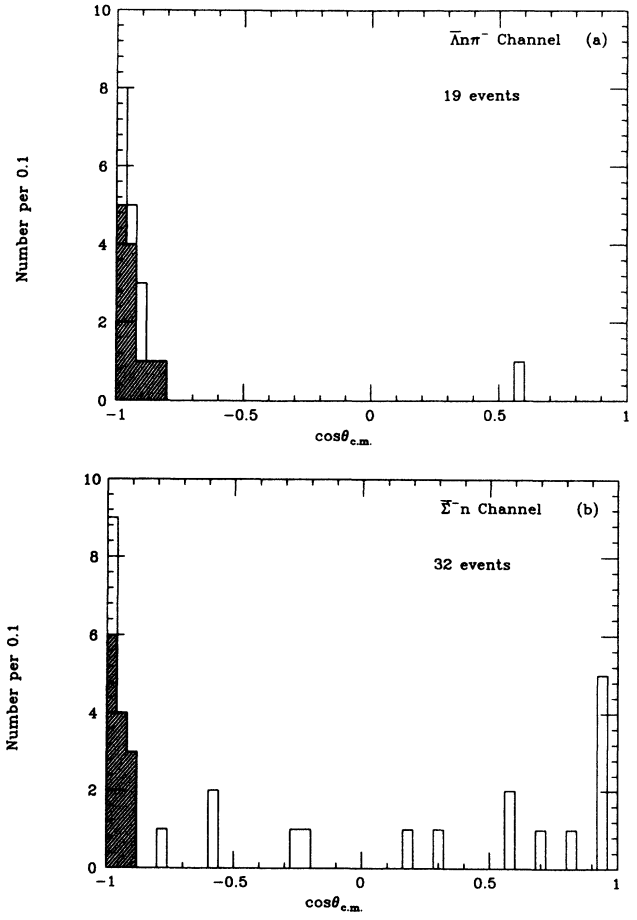

FIG. 8. c.m. production cosine for T-diquonium sample. Shaded part of the histogram indicates those events surviving the kinematic cut on K^0 momenta. (a) $\bar{\Lambda}n\pi^-$ channel. (b) $\bar{\Sigma}^-n$ channel.

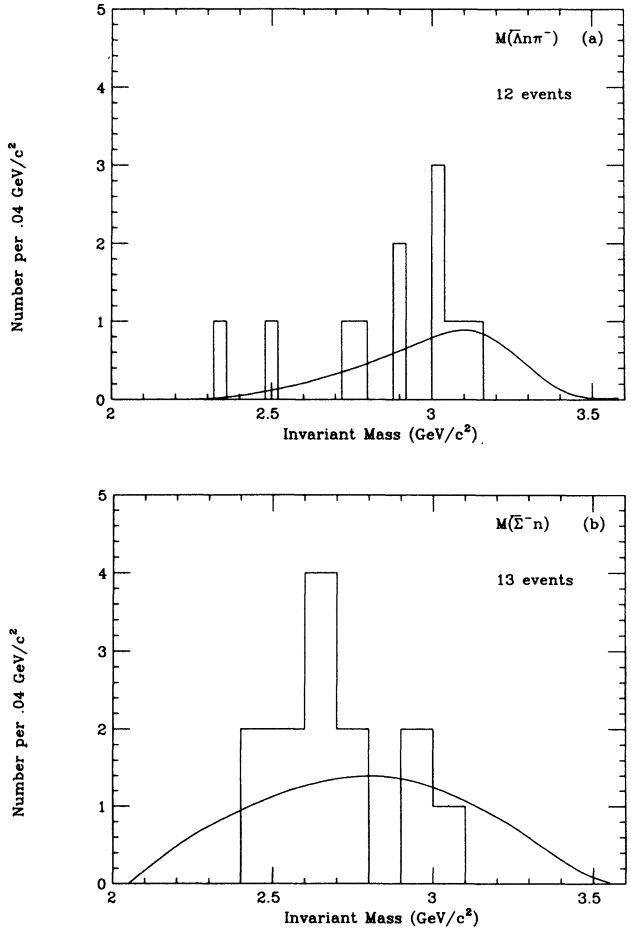

FIG. 9. Invariant masses for T-diquonium sample surviving all cuts. Monte Carlo–generated background curves are superimposed. (a) $\bar{\Lambda}n\pi^-$ channel. (b) $\bar{\Sigma}^-n$ channel.

al events) which has the largest excess of events above the smooth background curve. We then assumed that these n_0 events originated from a signal s plus a background b, where b was determined from the phase-space considerations above. We determined the mean value μ for a Poisson distribution which would give a probability of 0.05 for getting the observed number or fewer counts in that bin. The 95% confidence limit for s was then given by $s=\mu-b$. Application of the acceptance criterion [by using the acceptance factors from Tables I and II on the $\bar{p}n\to K^0$ (inclusive) sensitivity value of 29.3 events/μb] yielded a sensitivity S (events/μb) for each channel. This value was divided into the confidence limit s obtained above to produce the cross-section upper limit. Inherent in our procedure is the assumption that the resonance width is considerably less than 160 MeV/c^2 for the $\bar{\Lambda}n\pi^-$ channel and 400 MeV/c^2 for the $\bar{\Sigma}^-n$ channel.

A similar procedure was followed for the three- and four-prong channels which remain. Application of the kinematic cut yielded only one event in the $\bar{\Sigma}^-p\pi^-$ channel, however, and no events in the other channels. Note that for the channels containing zero events, $n_0=b=0$ and $s=\mu$. For simplicity, the upper limits were applied to the entire mass range of interest ($2.2\le M_X\le 3.6$ GeV/c^2). In Table V we exhibit a summary of the individual channel sensitivities and the $\Gamma\sigma$ 95% confidence limit for the backward-produced $I=\frac{3}{2}$ T-diquonium. A representative value for these channels would be 0.9 μb.

In summary, a survey of several exclusive mass distributions ($\bar{\Lambda}n\pi^-$, $\bar{\Sigma}^-n$, $\bar{\Lambda}p\pi^-\pi^-$, $\bar{\Sigma}p\pi^-$, and $\bar{\Sigma}^{\pm}n\pi^{\mp}\pi^-$) in the reaction $\bar{p}n\to\bar{K}^0_fX^-$ at 8.9 GeV/c, found no evidence of the SU(3) exotic states in the mass range 2.2–3.6 GeV/c^2. (The particular configuration of our trigger did not permit an analysis of semi-inclusive or inclusive mass distributions.) Ninety-five percent confidence limits were found in the range 0.50–1.63 μb for the various channels. We have argued that the $\bar{p}n$ reaction channels are favored for $Q^2\bar{Q}^2$ production in the backward direction assuming asymptotic planarity and the color-singlet hypothesis. Our upper limit values for exotic $Q^2\bar{Q}^2$ production are consistent with the cross sections for the cryptoexotic multiplet observed by Azooz and collaborators mentioned earlier. In fact, our limits are comparable with those obtained in the other planar processes $\pi^+p\to n_fZ^{++}$ by Alam *et al.*, $\pi^+p\to\Lambda_fX^{++}$ by Baltay *et al.*, and $\bar{p}n\to\pi^+_fZ^{--}$ by Azooz *et al.*, but are approximately an order of magnitude larger than those set in the $\pi^-n\to p_fZ^{--}$ search.[31] Finally, though our limits are of the same order of magnitude as cross sections of the U multiplet discussed earlier, the production mechanisms are quite different, precluding a direct comparison with our results.

TABLE V. Channel sensitivities and 95%-confidence-level upper limits on cross section × branching ratio for the mass range $2.2\le M_X\le 3.6$ GeV/c^2.

Channels	S (events/μb)	95%-C.L. upper limits (μb)
$\bar{\Lambda}n\pi^-$	6.8	1.23
$\bar{\Sigma}^-n$	7.4	1.63
$\bar{\Lambda}p\pi^-\pi^-$	6.0	0.68
$\bar{\Sigma}^-p\pi^-$	6.5	0.50
$\bar{\Sigma}^{\pm}n\pi^{\mp}\pi^-$	5.3	0.57

ACKNOWLEDGMENTS

We gratefully acknowledge the staff of the 40-inch Bubble-Chamber Group at SLAC for all of their assistance before and during our run. We would especially like to thank Knut Skarpaas for designing the iron frame of the calorimeter, Clive Field for his help with our trigger and the proportional wire chambers, and Dieter Freytag for his help with the SHF analysis system. We would like to acknowledge Art Leino for his help with the SHF on-line data-acquisition software which was adapted for use with this experiment. We would like to acknowledge Richard Kass and P. F. Lang for participating during the early part of the experiment. There are also a number of people to thank who were associated with the Bubble-Chamber Group at SLAC and lent assistance and advice when needed: Jon Levin, Jim Mueller, Ross Aintablian, Victor Cautis, and Jean-Paul Porte. This research was sponsored, in part, by the Department of Energy.

*Current address: Physics Department, California State University, Sacramento, California 95189.

†Deceased.

[1]M. S. Alam *et al.*, Phys. Lett. **53B**, 207 (1974); C. Baltay *et al.*, *ibid.* **57B**, 293 (1975); F. Azooz *et al.*, Nucl. Phys. **B244**, 277 (1984); J. Boucrot *et al.*, *ibid.* **B121**, 251 (1977); R. M. Bionta *et al.*, Phys. Rev. Lett. **46**, 970 (1981); H. Brundiers *et al.*, Phys. Lett. **64B**, 107 (1976).

[2]J. Rosner, Phys. Rev. Lett. **22**, 689 (1969).

[3]G. F. Chew, in *Asymptotic Realms of Physics: An M.I.T. Symposium in Honor of Francis Low,* edited by Alan H. Guth (MIT Press, Cambridge, MA, 1983), p. 49.

[4]H. Chan and H. Høgaasen, Phys. Lett. **72B**, 121 (1977); M. B. Gavela *et al.*, *ibid.* **79B**, 459 (1978); A. W. Hendry and I. Hinchcliffe, Phys. Rev. D **18**, 3453 (1978); R. L. Jaffe, *ibid.* **17**, 1444 (1978); C. S. Kalman, Lett. Nuovo Cimento **25**, 133 (1979).

[5]H. Chan and H. Høgaasen, Nucl. Phys. **B136**, 401 (1978).

[6]The QQ combination is repulsive in the color-sextet state if it is attractive in the triplet state, and the separation of the quarks will not be great enough to prevent $Q\bar{Q}$ pairings.

[7]R. L. Jaffe, Phys. Rev. D **15**, 267 (1977). Note that mesonium decays could have sufficiently narrow widths if the decays are just above threshold. Some support for such resonances can be found in $\gamma\gamma\to\rho^0\rho^0$ and $\gamma\gamma\to\gamma\rho^0\rho^0$ reactions in the mass region 1.45–1.65 GeV/c^2 (100–200 MeV/c^2 above threshold) with $\Gamma=200\pm100$ MeV/c^2. [See K. F. Liu, in *Hadron Spectroscopy—1985,* proceedings of the International

Conference, College Park, Maryland, 1985, edited by S. Oneda (AIP Conf. Proc. No. 132) (AIP, New York, 1985), p. 272].

[8]B. Nicolescu, Nucl. Phys. **B134**, 495 (1978).

[9]F. Azooz *et al.*, Phys. Lett. **122B**, 471 (1983). Also P. Benkheiri *et al.* [*ibid.* **68B**, 483 (1977)] report cross sections of the order of 10–30 nb for $\pi^- p \to p\pi^- p\bar{p}$ at 9 and 12 GeV.

[10]M. Bourquin *et al.*, Phys. Lett. B **172**, 113 (1986).

[11]K. J. Barnes, P. Forgacs, and M. T. Vaughn, Phys. Lett. B **182**, 208 (1986).

[12]Note that the direct production of $QQ\overline{QQ}$ states with unconventional quantum numbers would require the crossing of two or more quark lines in quark line diagrams for available beams and targets.

[13]R. Davis *et al.*, Nucl. Phys. **B96**, 426 (1975); C. Evangelista *et al.*, *ibid.* **B184**, 189 (1981); G. Giacomelli *et al.*, Phys. Lett. **33B**, 373 (1970).

[14]See Ref. 1.

[15]This conclusion rests on the assumptions that the color-mixing force originates only from the magnetic component and is short ranged (see G. H. N. Shoemaker, Ph.D. thesis, University of California, Davis, 1983).

[16]This is due primarily to the good efficiency at which antihyperons are identified in the bubble chamber.

[17]F. Azooz *et al.*, Nucl. Phys. **B244**, 277 (1984).

[18]This is contrasted with the much higher probability for M-diquonium ($M_4 \to MM_4$) for forward M_4 production in MB scattering, since the forward production mechanism involves the exchange of a $QQ\overline{QQ}$ trajectory at $t<0$. This trajectory can be regarded as a mixture of l states (especially $l=0$). Therefore, there is nothing to inhibit gluon exchange between the diquarks. Chan and Høgaasen (Ref. 5) also suggest additional mechanisms for M-diquonium forward production.

[19]This is due to the centrifugal barrier for the orbiting diquarks.

[20]Chan and Høgaasen (Ref. 5), Fig. 3, p. 409. They proposed a model of the baryonium spectrum where the diquonium masses are split due to color-magnetic gluon exchange. For our multiplet an $l=2$ state lies close to $N\bar{\Sigma}$ and an $l=3$ to the $\Delta\bar{\Lambda}$ threshold. The larger orbital angular momentum enhances the probability of baryonium decays.

[21]G. H. N. Shoemaker *et al.*, Nucl. Instrum. Methods Phys. Res. A **243**, 374 (1986).

[22]See Ref. 21.

[23]This gate would accept events where signal overlap occurred within 40 nsec of the previous trigger (where the analog contribution to the next trigger was expected to be small).

[24]W. Michael, G. L. Harris, and D. G. Knierim, University of California at Davis Report No. UCID-38 80, 1981 (unpublished).

[25]For high-momentum particles, minimum-ionizing particles dominate the shower and the average multiplicity of these increases almost linearly with incident energy.

[26]Shoemaker *et al.* (Ref. 21), Fig. 9.

[27]Shoemaker *et al.* (Ref. 21).

[28]The t distribution of the T-diquonium candidates alone was checked and found to be similar to the K^0 inclusive sample; the latter, however, provided more statistics and, consequently, a better parametrization.

[29]This condition was chosen to minimize the influence of accidentals due to cosmic rays and beam contamination (see Sec. IV B).

[30]The phase-space distributions include both kinematic and acceptance cuts.

[31]See Ref. 1.

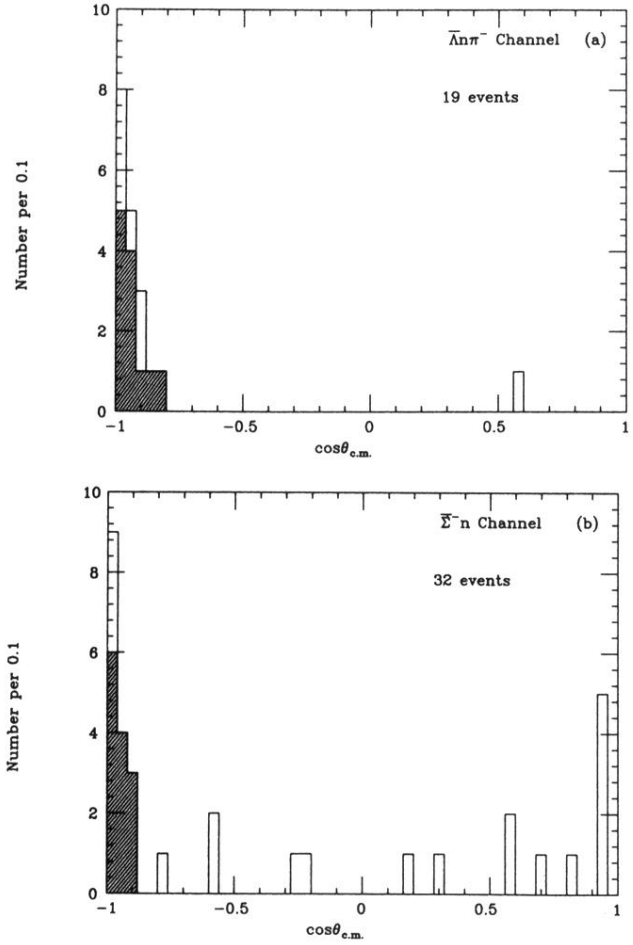

FIG. 8. c.m. production cosine for T-diquonium sample. Shaded part of the histogram indicates those events surviving the kinematic cut on K^0 momenta. (a) $\bar{\Lambda}n\pi^-$ channel. (b) $\bar{\Sigma}^-n$ channel.